Procedia Computer Science

Volume 29, 2014, Pages 811–820

ICCS 2014. 14th International Conference on Computational Science

Fast Low-Fidelity Wing Aerodynamics Model for Surrogate-Based Shape Optimization

Leifur Leifsson[1*], Slawomir Koziel[1†], and Adrian Bekasiewicz[2‡]

[1]*Reykjavik University, Iceland*

[2]*Gdansk University of Technology, Poland*

leifurth@ru.is, koziel@ru.is, adrian.bekasiewicz@eti.pg.gda.pl

Abstract

Variable-fidelity optimization (VFO) can be efficient in terms of the computational cost when compared with traditional approaches, such as gradient-based methods with adjoint sensitivity information. In variable-fidelity methods, the direct optimization of the expensive high-fidelity model is replaced by iterative re-optimization of a physics-based surrogate model, which is constructed from a corrected low-fidelity model. The success of VFO is dependent on the reliability and accuracy of the low-fidelity model. In this paper, we present a way to develop a fast and reliable low-fidelity model suitable for aerodynamic shape of transonic wings. The low-fidelity model is component based and accounts for the zero-lift drag, induced drag, and wave drag. The induced drag can be calculated by a proper method, such lifting line theory or a panel method. The zero-lift drag and the wave drag can be calculated by two-dimensional flow model and strip theory. Sweep effects are accounted for by simple sweep theory. The approach is illustrated by a numerical example where the induced drag is calculated by a vortex lattice method, and the zero-lift drag and wave drag are calculated by MSES (a viscous-inviscid method). The low-fidelity model is roughly 320 times faster than a high-fidelity computational fluid dynamics models which solves the Reynolds-averaged Navier-Stokes equations and the Spalart-Allmaras turbulence model. The responses of the high- and low-fidelity models compare favorably and, most importantly, show the same trends with respect to changes in the operational conditions (Mach number, angle of attack) and the geometry (the airfoil shapes).

Keywords: Aerodynamic wing design, shape optimization, variable-fidelity modeling, low-fidelity modeling, transonic wing.

* Engineering Optimization & Modeling Center, School of Science and Engineering

† Engineering Optimization & Modeling Center, School of Science and Engineering

‡ Faculty of Electronics, Telecommunications and Informatics

Selection and peer-review under responsibility of the Scientific Programme Committee of ICCS 2014

© The Authors. Published by Elsevier B.V.
doi:10.1016/j.procs.2014.05.073

1 Introduction

The use of optimization methods in the aerodynamic design process has now become commonplace (Leoviriyakit *et al*., 2003; Braembussche, 2008). The use of high-fidelity methods, coupled with optimization techniques, has led to improved design efficiency. Although simulation-driven aerodynamic design optimization has progressed much in the last decades, it still involves numerous challenges. One of the biggest issues is that high-fidelity computational fluid dynamics (CFD) simulations are computationally expensive. At the same time, conventional optimization techniques usually require a large number of simulations. Therefore, direct design optimization of high-fidelity models using traditional gradient-based techniques can be prohibitive, even with adjoint sensitivity information (Jameson, 1988).

Variable-fidelity optimization (VFO) methods have shown to be efficient and can offer significant savings in computational cost (Forrester and Keane, 2009; Koziel, Echevaerríam, and Leifsson, 2011; Alexandrov *et al*., 2000; Robinson *et al*., 2008). VFO replaces the direct optimization of an accurate, but computationally expensive, high-fidelity CFD model by an iterative re-optimization of a physics-based surrogate model. The physics-based surrogate model is comprised of a low-fidelity model (e.g., a simplified physics model, or coarse discretization CFD model) and a proper response correction (e.g., space mapping (Jonsson, Leifsson, and Koziel, 2013), shape-preserving response prediction (Koziel and Leifsson, 2013)).

The success of VFO hinges on the properties of the surrogate model. In particular, the low-fidelity model must exhibit the same trends as the high-fidelity model with respect to any design parameter change. In this paper, we present a way to develop a fast and reliable low-fidelity model for evaluating the aerodynamic performance of a wing in transonic flow. The low-fidelity model is suitable for use in surrogate-based aerodynamic shape optimization. We present a numerical example involving the aerodynamic analysis of a swept transonic wing using a high-fidelity CFD model and the proposed low-fidelity model. The results show that the correspondence between the two models is excellent.

2 Wing Aerodynamic Design

2.1 Problem Formulation

In general, aerodynamic design of wing shapes can be formulated as a constrained nonlinear minimization problem of the following form

$$\boldsymbol{x}^* = \arg\min_{\boldsymbol{x}} H(f(\boldsymbol{x})), \quad \text{s.t. } g_j(\boldsymbol{x}) \le 0,\ h_k(\boldsymbol{x}) = 0,\ \boldsymbol{l} \le \boldsymbol{x} \le \boldsymbol{u}, \tag{1}$$

where H is the objective function, $f(\boldsymbol{x})$ is the aerodynamic model, $\boldsymbol{x}$ is the design variable vector, $g_j(\boldsymbol{x})$ are the inequality constraints with $j = 1,\ldots,M$, $h_k(\boldsymbol{x})$ are the equality constraints with $k = 1,\ldots,N$, and $\boldsymbol{l}$ and $\boldsymbol{u}$ are the lower and upper bounds of the design variables, respectively.

The function f stands for a high-fidelity wing aerodynamic model, typically representing non-dimensional aerodynamic forces, such as the lift and drag coefficients. For example, we can have $f(\boldsymbol{x}) = [C_{L.f}(\boldsymbol{x})\ C_{D.f}(\boldsymbol{x})]^T$, where $C_{L.f}$ and $C_{D.f}$ are the (high-fidelity CFD-simulated) wing lift and drag coefficients, respectively. For drag minimization, the objective function can take the form $H(f(\boldsymbol{x})) = C_{D.f}(\boldsymbol{x})$ with a lift constraint of the form $h_1(f(\boldsymbol{x})) = C_{L.f}(\boldsymbol{x}) - C_{L.\text{target}} = 0$, where $C_{L.\text{target}}$ is a target lift coefficient. Other constraints could be included. For example, a minimum pitching moment or a maximum allowable section lift coefficient.

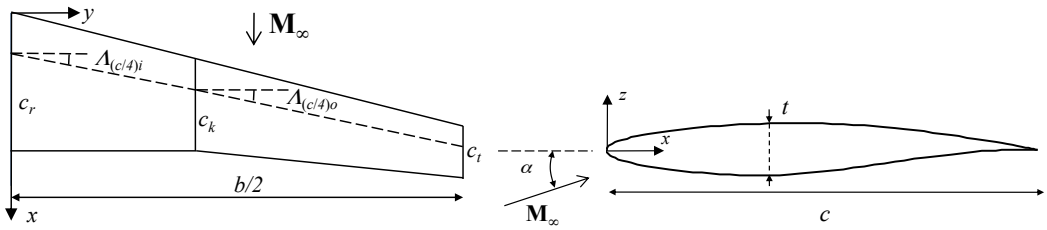

(a) (b)

Figure 1: Elements of a clean wing shape: (a) planform view, (b) an airfoil section.

The components of $\boldsymbol{x}$ are the wing geometry parameters, such as the planform shape (typically, the span b, quarter-chord sweep $\Lambda_{c/4}$, section chords c_i (i = root, kink, and tip), and the kink location; see Fig. 1(a)) and the airfoil shapes at different spanwise locations (Fig. 1(b)). The airfoil shapes can be described by various parameterization methods, such as B-spline curves (Lepine *et al*., 2001), Bezier-PARSEC (Rogalsky and Derksen, 2009), and Hicks-Henne bump functions (Hicks and Henne, 1978), each with various degrees of freedom. The angle of attack α can also be taken as a design variable, or adjusted during the simulation to obtain the required lift.

We note here that evaluating a high-fidelity CFD model may be computationally expensive. Therefore, straightforward attempts to solve (1) may be infeasible, especially if the design space is large. Even with adjoint sensitivity information (Jameson, 1988) direct optimization of the high-fidelity model may still be impractical.

2.2 Surrogate-based Optimization

Surrogate-based optimization (SBO) has been shown to accelerate the design process significantly. In general, the SBO approach does not attempt to solve the original problem (1) directly. Instead, a sequence of approximate solutions are generated, $\boldsymbol{x}^{(i)}$, $i = 0, 1, \ldots$, ($\boldsymbol{x}^{(0)}$ is the initial design) as

$$\boldsymbol{x}^{(i+1)} = \arg\min_{\boldsymbol{x}} H(s^{(i)}(\boldsymbol{x})), \tag{2}$$

where H is a given objective function and $s^{(i)}(\boldsymbol{x})$ is the surrogate model at iteration i. The flow of a generic SBO algorithm is shown in Fig. 2. Provided that the surrogate model is adequately formulated and constructed, the SBO approach can yield, in many cases, a satisfactory design at the cost of only a few high-fidelity model evaluations. The design acceleration is dependent on the cost of constructing the surrogate model.

One way of constructing the surrogate model is by using a variable-fidelity approach. Here, the surrogate model is comprised of a low-fidelity model, $c(\boldsymbol{x})$, and a suitable correction. In aerodynamic analysis, there are several correction techniques available, such as the shape-preserving response prediction, space mapping, and the adaptive response correction. The low-fidelity model is a fast representation of the high-fidelity one and can be based on any underlying model which captures the main physics of the problem. The low-fidelity model can be developed using, for example, simplified physics models, or coarse discretization CFD models. However, the low-fidelity model has to exhibit similar response changes as the high-fidelity model. For example, if the objective function increases due to a certain change in the design variables, the low-fidelity model has to increase as well. It does not have increase by the same amount, but only show the same trend.

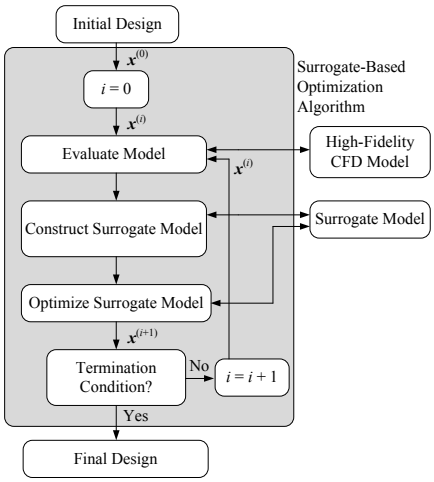

Figure 2: Flow of a generic surrogate-based optimization (SBO) algorithm.

3 Low-fidelity Model

The low-fidelity model is defined as

$$c(\boldsymbol{x}) = [C_{L.c}(\boldsymbol{x}) \quad C_{D.c}(\boldsymbol{x})], \tag{3}$$

where $C_{L.c}(\boldsymbol{x})$ and $C_{D.c}(\boldsymbol{x})$ are the wing lift and drag coefficients, respectively. The model $c(\boldsymbol{x})$ is a computationally cheap representation of the high-fidelity one. In order to be suitable for the surrogate-based optimization process, the low-fidelity model has to adequately account for the main features of the high-fidelity one, including its overall trends, i.e., the changes of the model responses as a result of any geometry and/or operating condition adjustments. For example, if a reduction in the wing thickness leads to a reduction in drag, then the same trend should be observed in the low-fidelity model. The amount by which the drag changes in both models may be different.

In this work, we follow a widely used approach (see, for example, Grasmeyer (1999)) by modeling the low-fidelity wing drag coefficient in a component-wise fashion as

$$C_{D.c}(\boldsymbol{x}) = C_{D0}(\boldsymbol{x}) + C_{Di}(\boldsymbol{x}) + C_{Dw}(\boldsymbol{x}), \tag{4}$$

where C_{D0} is the zero-lift drag coefficient, C_{Di} is the induced drag coefficient, and C_{Dw} is the compressibility drag coefficient. The zero-lift drag coefficient, estimated at zero lift, provides an estimate of the surface friction drag and the pressure drag due to the wing form. The induced drag coefficient yields an estimate of the drag due to lift. Drag due to pressure shocks is represented by the compressibility drag coefficient. Each component of the low-fidelity model needs to be modeled appropriately to capture the main behavior of the high-fidelity model with respect to any changes in the model parameters, such as the operating condition and the design variables. The low-fidelity wing lift coefficient is set equal to the high-fidelity wing lift coefficient, i.e., $C_{L.c} = C_{L.f}$.

We propose the following way of estimating each component of (4). The zero-lift coefficient is modeled by the strip theory (see, for example, Mason (1990)) where the planform is divided into several stream-wise strips and the sum of the contribution of each strip yields the total wing drag coefficient as

$$C_{D0}(\boldsymbol{x}) = \sum C_{d0}(\boldsymbol{x}) \frac{S_{strip}}{S_{ref}}, \tag{5}$$

where C_{d0} is the strip section zero-lift drag coefficient, S_{strip} is the area of the strip, and S_{ref} is the planform reference area. The section zero-lift drag coefficient is calculated using a two-dimensional CFD model. The induced drag coefficient is calculated using a vortex lattice method (VLM) (see, for example, Grasmeyer (1997)). The input to the VLM analysis is the planform shape and the wing lift coefficient ($C_{L.c} = C_{L.f}$). The VLM analysis will yield the induced drag (C_{Di}), as well as the corresponding wing spanload distribution. Now, the compressibility drag coefficient is calculated in a similar way as the zero-lift drag coefficient, but using the lift coefficient distribution from the VLM analysis as an input to the two-dimensional CFD analysis of each spanwise strip. The compressibility drag coefficient is, therefore, calculated as

$$C_{Dw}(\boldsymbol{x}) = \sum C_{dw}(\boldsymbol{x}) \frac{S_{strip}}{S_{ref}}, \tag{6}$$

where C_{dw} is the strip section compressibility drag coefficient.

Simple sweep theory (see, for example, Mason[31]) is used to account for wing sweep effects. For each strip, the CFD analysis is performed at a Mach number $M_n = M_\infty \cos\Lambda_{c/4}$ (where M_∞ is the free-stream Mach number and $\Lambda_{c/4}$ is the strip quarter-chord sweep angle), at a chord length $c_n = c \cos\Lambda_{c/4}$ (c is the strip chord length) and thickness-to-chord ratio $(t/c)_n = (t/c)/\cos\Lambda_{c/4}$ ((t/c) is the strip thickness-to-chord ratio).

4 Numerical Example

In this example, we compare a high-fidelity wing aerodynamic model with the proposed low-fidelity modeling approach. In particular, we consider the transonic flow past a well-recognized transonic wing, and investigate the model responses when the operational conditions, as well as the geometry, are changed.

4.1 Problem Setup

We consider the ONERA M6 wing which has a swept trapezoidal shape with constant airfoil profile. The wing and airfoil shape is shown in Fig. 3. The semi-span is $b/2$ = 1.1963 m, root chord length is c_r = 0.8059 m, the leading edge sweep is Λ = 30 deg, the taper ratio is $\lambda = c_t/c_r$ = 0.562, and the aspect ratio is AR = 3.8.

4.2 High-fidelity Model

The flow is assumed to be steady, viscous, and adiabatic with no body forces. We solve the Reynolds-averaged Navier-Stokes equations with the one equation Spalart-Allmaras turbulence model.

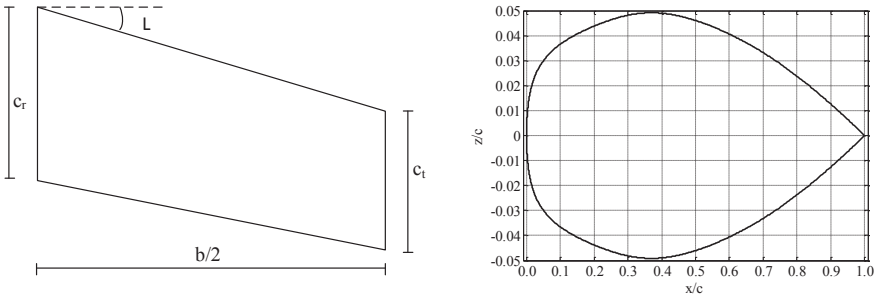

Figure 3: The ONERA M6 wing and airfoil shape.

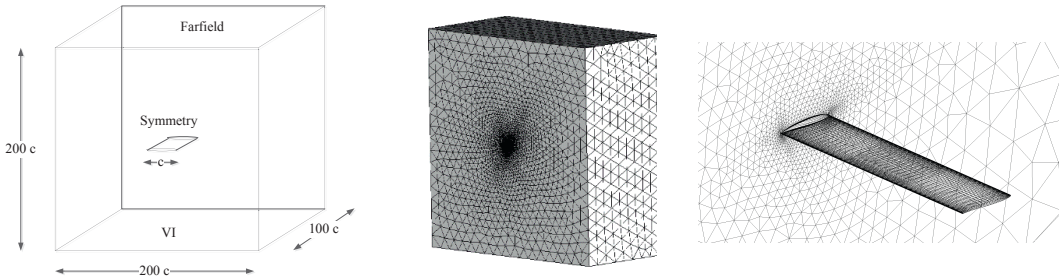

(a) (b) (c)

Figure 4: Three-dimensional wing CFD model: (a) the solution domain and boundary conditions, and an example three-dimensional computational mesh, (b) the farfield, and (c) a close-up of the wing surface.

The farfield is configured in a box-topology where the airfoil/wing geometry is placed in the center of the box. The leading edge is placed at the origin, with the farfield extending 100 chord lengths away from the origin in every direction. To reflect the compressible nature of this problem, two types of boundaries are used. The pressure-farfield is applied to the boundary on all surfaces, except where the wing penetrates the symmetry boundary. A sketch of the setup in three-dimensions is shown in Fig. 4(a).

An unstructured tri/tetra shell grid is created on all surfaces. The shell grid from the wing is then extruded into the volume where the volume is flooded with tri/tetra elements. The grid is made dense close to the wing where it then gradually grows in size as moving away from the wing surfaces. To capture the viscous boundary layer an inflation layer or a prism layer is created on the wing surfaces as well. In the stream-wise direction, the number of elements on the wing is set to 100 on both upper and lower surface. The bi-geometric bunching law with a growth ratio of 1.2 is employed in the stream-wise direction over the wing to obtain a denser element distribution at the leading edge and the trailing edge. This is done in order to capture the high pressure gradient at the leading edge and the separation at the trailing edge. The minimum element size of the wing in the stream-wise direction is set to 0.1%c, where c is the wing chord length, and it is located at the leading and trailing edge. The elements in the span-wise direction are distributed uniformly and number of elements set to 100 over the semi-span. A prism layer is used to capture the viscous boundary layer. This layer consists of a number of structured elements that grow in size normal to the wing surface into the domain volume. The inflation layer has an initial height of $5 \times 10^{-6}c$ where it is grown 20 layers into the volume using an exponential growth law with ratio of 1.2. The initial layer height is chosen so that $y^+ < 1$ at all nodes on the wing. Example grid is shown in Figs. 4(b) and 4(c).

The flow solver is an implicit density-based one using the Roe-FDS flux type. The spatial discretization schemes are set to second order for all variables, and the gradient information is found using the Green-Gauss node based method. The residuals, which are the sum of the L^2 norm of all

governing equations in each cell, are monitored and checked for convergence. The convergence criterion for the high-fidelity model is such that a solution is considered to be converged if the residuals have dropped by six orders of magnitude, or the total number of iterations has reached 1,000. The lift and drag coefficients are obtained by integrating the pressure and skin friction coefficients over the surface of the wing. The grid parameters were obtained by a grid independence study. The grid has approximately 4 million cells and the wall-clock simulation time is approximately 13.5 hours.

4.3 Low-fidelity Model

The low-fidelity model is setup as described in Section 3. The wing is divided uniformly into six strips. The induced drag coefficient, C_{Di}, is calculated using a vortex lattice code (see, e.g., Grasmeyer (1997)). The zero-lift and wave drag coefficients, C_{D0} and C_{Dw}, respectively, are calculated using MSES (Drela and Giles, 1987).

MSES is a viscous-inviscid analysis method capable of calculating transonic and low Reynolds number airfoil flows. The Euler equations are discretized on a conservative streamline grid and are strongly coupled to a two-equation integral boundary-layer formulation using the displacement thickness concept. A transition prediction formulation is incorporated into the viscous formulation. The entire discrete equation set, including the viscous and transition formulations, is solved as a fully coupled nonlinear system by a global Newton method. The method is rapid and can handle strong viscous-inviscid interactions, such as shock-induced separation. In this work, MSES is utilized in the viscous-inviscid analysis mode with fixed transition. A typical evaluation time is roughly 15 sec. The overall wall-clock simulation time of the low-fidelity model approximately 2.5 min. The ratio of simulation times of the high- to low-fidelity models is roughly 320.

4.4 Effects of Variation in the Operating Conditions for a Fixed Geometry

The drag polar of the ONERA M6 at Mach = 0.8395 is shown in Fig. 5(a). One can observe that the drag polars of each model are similar. The low-fidelity model predicts lower drag than the high-fidelity one for a given lift. Furthermore, the minimum drag value is obtained at different lift values for each model. The variation of the drag coefficient with Mach number at a constant lift is shown in Fig. 5(b). The low-fidelity model follows the high-fidelity one, but is shifted in drag values.

4.5 Effects of Variation in the Geometry at a Fixed Operating Condition

Several wing shapes were generated by perturbing (moderately) the original ONERA M6 wing. The airfoil shapes are shown in Fig. 6. Flow analyses of the wings were performed at both low and high lift coefficient values. The results are shown in Fig. 7. The low-fidelity model drag values follow the high-fidelity model quite well, i.e., the same trend in variation of the drag is observed in both models.

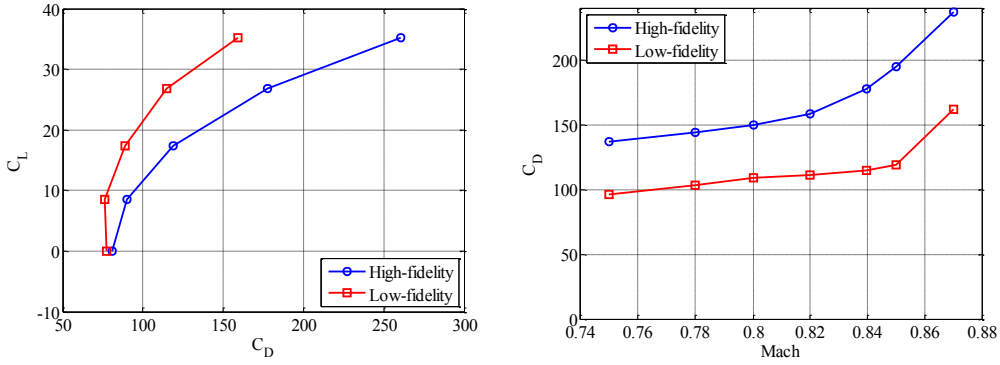

(a) (b)

Figure 5: Variation of the operating conditions for the ONERA M6 wing showing (a) the drag polar at Mach = 0.8395, and (b) variation of the drag coefficient with Mach number at constant lift coefficient ($C_L \approx 26$ cts).

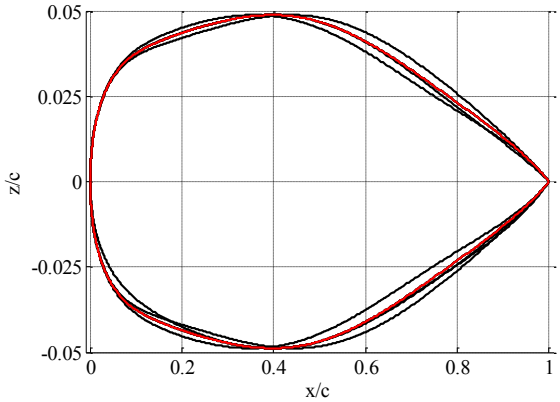

Figure 6: Original (red) and perturbed (black) ONERA M6 wing airfoil shapes.

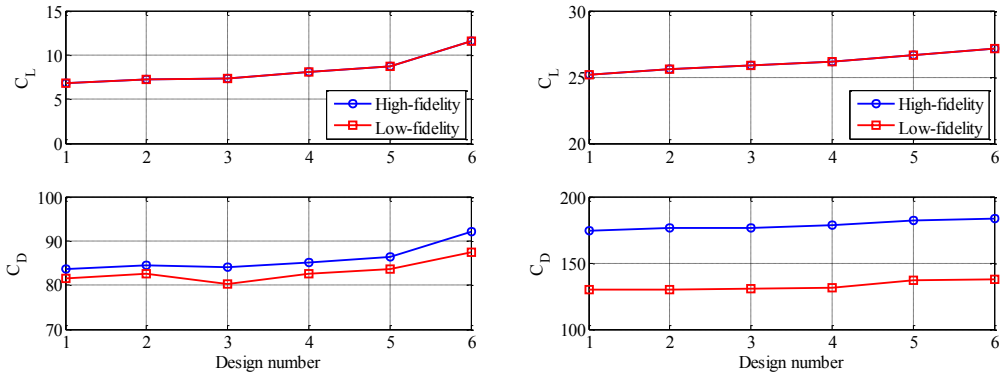

(a) (b)

Figure 7: Lift and drag coefficients for several perturbed designs of the ONERA M6 wing for (a) Mach = 0.80 and angle of attack of 1 deg, and (b) Mach = 0.84 and angle of attack of 3 deg

5 Conclusion

We have presented a methodology for constructing a fast and reliable low-fidelity model appropriate for the aerodynamic shape optimization of transonic wings. The low-fidelity model is applicable to three-dimensional wings but employs fast two-dimensional flow models and strip theory. The numerical example illustrates that a low-fidelity model faster by two-orders of magnitude than a typical three-dimensional model can be obtained. Moreover, the low-fidelity model exhibits the same trends as the high-fidelity model with respect to any design space parameter changes. The utilization of the proposed low-fidelity model in aerodynamic shape optimization may lead to substantial computational savings.

References

Alexandrov, N.M., Lewis, R.M., Gumbert, C.R., Green, L.L., and Newman, P.A. (2000) *Optimization with Variable-Fidelity Models Applied to Wing Design.* 38th Aerospace Sciences Meeting & Exhibit, Reno, NV, AIAA Paper 2000-0841.

Braembussche, R.A., (2008) *Numerical Optimization for Advanced Turbomachinery Design.* In *Optimization and Computational Fluid Dynamics*, Thevenin, D. and Janiga, G., editors, Springer, pp. 147-189.

Drela, M., and Giles, M.B. (1987) *Viscous-Inviscid Analysis of Transonic and Low Reynolds Number Airfoils*. AIAA Journal, vol. 25, no. 10,pp. 1347-1355.

Forrester, A.I.J., and Keane, A.J. (2009) *Recent advances in surrogate-based optimization.* Prog. in Aerospace Sciences, vol. 45, no. 1-3, pp. 50-79.

Grasmeyer, J.M., (1997) *A Discrete Vortex Method for Calculating the Minimum Induced Drag and Optimum Load Distribution for Aircraft Configurations with Noncoplanar Surfaces*. VPI-AOE-242, Department of Aerospace and Ocean Engineering, Virginia Polytechnic Institute and State University, Blacksburg, Virginia, 24061.

Grasmeyer, J.M. (1999) *Multidisciplinary Design Optimization of a Transonic Strut-Braced Wing Aircraft.* 37th AIAA Aerospace Sciences Meeting and Exhibit, Reno, NV, AIAA Paper 99-001.

Hicks, R.M., and Henne, P.A. (1978) *Wing Design by Numerical Optimization.* Journal of Aircraft, Vol. 15, No. 7, pp. 407-412.

Jameson, A., (1988) *Aerodynamic Design via Control Theory.* Journal of Scientific Computing, Vol. 3, pp. 233-260.

Jonsson, E., Leifsson, L., and Koziel, S. (2013) *Aerodynamic Optimization of Wings by Space Mapping.* 51st AIAA Aerospace Sciences Meeting including the New Horizons Forum and Aerospace Exposition, Grapevine, Texas, January 7-10.

Koziel, S., Echeverría-Ciaurri, D., and Leifsson, L. (2011) *Surrogate-based methods.* In S. Koziel and X.S. Yang (Eds.) *Computational Optimization, Methods and Algorithms*, Series: Studies in Computational Intelligence, Springer-Verlag, pp. 33-60.

Koziel, S., and Leifsson, L. (2013) *Surrogate-Based Aerodynamic Shape Optimization by Variable-Resolution Models.* AIAA Journal, vol. 51, no. 1, pp. 94–106.

Lepine, J., Guibault, F., Trepanier, J.-Y., and Pepin, F. (2001) *Optimized Nonuniform Rational B-Spline Geometrical Representation for Aerodynamic Design of Wings*. AIAA Journal, Vol. 39, No. 11, pp. 2033-2041.

Leoviriyakit, K., Kim, S., and Jameson, A. (2003) *Viscous Aerodynamic Shape Optimization of Wings including Planform Variables.* 21st Applied Aerodynamics Conference, Orlando, Florida, June 23-26.

Mason, W.H., (1990) *Analytic Models for Technology Integration in Aircraft Design.* AIAA-90-3262.

Robinson, T.D., Eldred, M.S., Willcox, K.E., and Haimes, R. (2008) *Surrogate-Based Optimization Using Multifidelity Models with Variable Parameterization and Corrected Space Mapping.* AIAA Journal, vol. 46, no. 11.

Rogalsky, T., Derksen,R.W. (2009) *Bézier–PARSEC parameterization for airfoil optimization.* Canadian Aeronautics and Space Journal, Vol. 55, No. 3, pp. 163-174